THE AMERICAN SOCIETY OF MECHANICAL ENGINEERS
345 E. 47th St., New York, N.Y. 10017

96-TA-60

A PRACTICAL METHOD FOR PREDICTING THE WINDMILLING CHARACTERISTICS OF SIMPLE TURBO JET ENGINES

Min Su Choi†, Jin Shik Lim†,
and Yong Shik Hong††

ABSTRACT

A practical method for predicting the windmilling performance of simple turbojet engines in flight has been developed. The method incorporates the available loss correlations and analyses to estimate the major engine component performance and requires only basic geometric data. For a given flight Mach number and ambient conditions the steady-state windmilling performance is obtained by equating the compressor input torque to the turbine output torque. The transient performance is obtained from the excess turbine output torque. The present method's predictions are compared to the available windmilling test data from a typical small simple turbojet engine. They show good agreement over a wide range of flight conditions. Thus, this method can be used during the preliminary design stage of an engine development when the detailed hardware geometry and the component performance data are not yet available.

NOMENCLATURE

A	inflow or outflow peth annulus area
A_i	inlet area
A_N	nozzle area
a	distance from the leading edge to the maximum camber location of the airfoil
C	absolute velocity of air
c or l	chord
C_D	drag coefficient
C_{Da}	annulus wall drag coefficient
C_{Dp}	profile drag coefficient
C_{Ds}	secondary loss drag coefficient
C_L	lift coefficient
C_x	axial velocity of air
C_w	tangential velocity of air
g_c	constant in the force equation
h	altitude
H	blade height
i	incidence angle
i_{opt}	optimum incidence angle
I_p	polar moment of inertia
J	mechanical equivalent of heat
k_r	kinetic energy loss coefficient for rotor
k_s	kinetic energy loss coefficient for stator
L_r	rotor energy loss
L_s	stator energy loss
L_i	incidence loss
M_a	flight Mach number.
$\dot{m}_a$	air mass flow rate
N	rotational rpm
P	pressure
Re	Reynolds number
r_H	hub radius
r_m	mean radius
r_T	tip radius
s	blade pitch
T	temperature
t	time
t_c	tip clearance
T_q	torque
U	rotational speed
V	flight speed
W	relative velocity of air
β	relative air angle

† Agency for Defense Development Daejon, Korea
†† Professor, Department of Aerospace Engineering INHA University 253, Yong-Hyun Dong, Nam-Gu Inchon 402-751, Korea.

Presented at the 1996 ASME Turbo Asia Conference
November 5–7, 1996 — Jakarta, Indonesia

β'	blade angle
γ	specific heats ratio of air
δ	deviation angle
ϵ	deflection angle
η	component efficiency
η_0	efficiency with zero tip clearance
θ	camber
λ	mean work done factor
ρ	air density
ω	angular velocity

Superscript

*	nominal condition

Subscript

a	ambient condition
i	inlet
in or 1	component inlet
N	exhaust nozzle
out or 2	component outlet
T	total or stagnation

1. INTRODUCTION

When a turbojet engine, in flight, experiences an engine flameout its rotational speed drops rapidly until a steady windmilling state is established. On the other hand, when a turbojet engine is exposed to the ram air, the engine rotor begins rotation and accelerates until a steady state windmilling speed is reached. Understanding and prediction of such windmilling characteristics is important in determining the engine starting system requirements.

Several methods are used to start turbojet engines. Typical methods include the use of a small auxiliary power unit (APU), windmill, and cartridge. Among these the windmill method is probably the simplest and requires no special accessory equipment.

While many part-load performance analyses and prediction methods for turbojet engines have been developed (Refs. (1), (2), (3), (4)), very few windmill performance prediction and analysis methods can be found in the literature. The main difficulty of windmilling performance prediction is due to the lack of published performance data of the major engine components (e.g. compressors and turbines) in the very low speed range where the windmilling often takes place.

The windmilling analysis for turbojet engines can be approached in three different ways. One is to generate correlations of the experimental windmilling data obtained from many different engines. Another is to use accurate performance maps for each engine component which covers the low speed range. Together with pressure loss data of other engine parts, a complete performance analysis can be done. The third approach is to utilize the available cascade data to estimate the compressor and turbine loss parameters to analyze the windmilling characteristics.

Morita and Sasaki(5) developed an in-flight engine restart model based on the engine start test data of an actual engine. No detailed component performance maps are required for this method. However, the predicted results were not generalized for other engine types.

Wallner and Welna(6) and Sobolewski and Farley(7) conducted tests of several turbojet engines under various windmilling conditions and developed some generalized correlations. This correlation method is also applicable to engines similar to the ones investigated.

A theoretical study of windmilling turbojet engine was made by Shou(8). Generalized curves which characterize the windmilling performance were obtained from experimental data of several turbojet engines. Again, the accuracy of the method is limited to those engines similar to the reference engines.

The objective of the present work was to investigate the physical mechanism of windmilling and to develop a practical prediction method which can be used in the early stages of engine development where few component test data are available.

2. CHARACTERISTICS OF WINDMILLING OPERATION

Windmilling of an engine results from the high dynamic pressure ambient air going through the engine, rotating the engine rotor. The rotational speed and the direction depend on the vector sum of the frictional torque and the aerodynamic torque which act on each rotor. The mass flow and the flow velocity through the engine depend on the flow area and the over-all pressure drop across the engine.

During the transient windmilling phase the axial compressor goes through turbine mode, frictional duct mode, and finally compressor mode as its speed increases. As shown in Fig.1 the compressor acts like a turbine when rotational speed is close to zero. As the speed increases to the point where tangential velocity component, C_w, at inlet become equal to that at the exit, no torque is acted on the compressor. Therefore, the compressor behaves like a frictional duct. However, at high rpm, the compressor regains its compressor mode. On the other hand, the air flow always expands and continues to deliver energy to the turbine. Unlike the fired engine operation no heat transfer is involved and the flow through the engine can be considered adiabatic. Therefore, although the total temperature varies through the compressor and the turbine, the total temperature at the engine exit remains same as that at the inlet.

3. CALCULATION PROCEDURE

The numerical calculation procedure is composed of two iteration loops (Figure 2). The inner loop is to determine the windmilling operation conditions of each component satisfying mass flow balance. But this operating condition means a torque imbalance between the compressor and the turbine. So, the final operating condition of each component can be found through the outer loop in which the excess torque of a turbine is calculated at each iteration step.

4. LOSS THROUGH AXIAL COMPRESSORS

According to Horlock[9] and Dixon[10], the stagnation pressure loss through axial compressor blade rows arises from three sources - the profile drag , the annulus wall drag, and the secondary flow effects. The profile drag coefficient C_{DP} can be obtained from Fig. 3 for various incidence angles $(i-i^*)/\epsilon^*$. The corresponding relative deflection ϵ/ϵ^* can also be obtained from

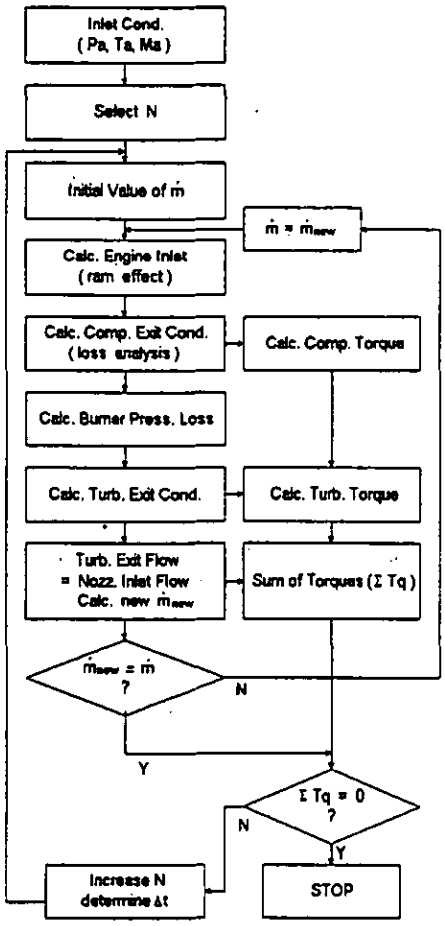

Figure 2: Calculation process flow chart.

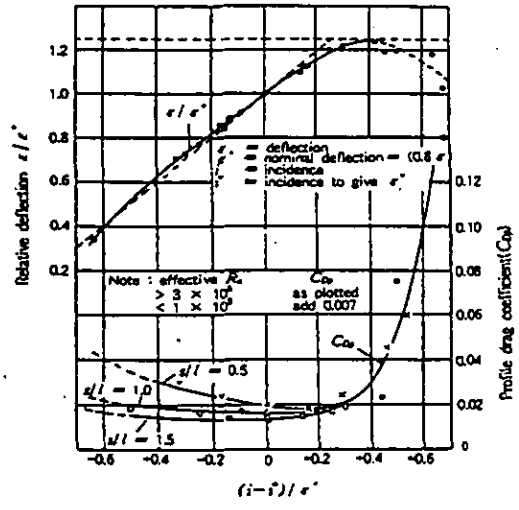

Figure 3: Off-design performance of a compressor cascade (9).

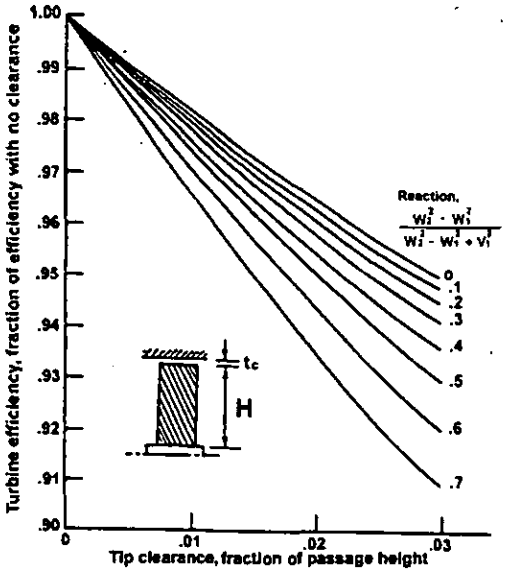

Figure 4: Effect of tip clearance fraction and degree of reaction on tip clearance loss (11).

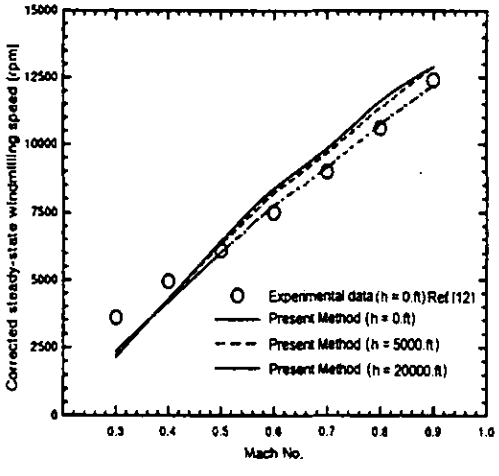

Figure 5: Effects of flight Mach number and altitude on steady state windmilling speed.

the same figure. The annulus wall drag coefficient C_{Da} and the secondary flow loss coefficient C_{Ds} may be estimated from Equations (1) and (2), respectively (Refs. (9), (10), (15)).

$$C_{Da} = 0.02\ (s/H) \tag{1}$$

$$C_{Ds} = 0.018\ C_L^2 \tag{2}$$

C_{Dp} is assumed to include a component for minimum tip clearance loss (Equation (2)). The sum of the three loss coefficients $C_D (= C_{Dp} + C_{Da} + C_{Ds})$ gives the total pressure loss ΔP_T and the stage efficiency η_{stage} (Steps 13&15 in Appendix A).

For a multi-stage compressor the performance calculation is made by stage stacking techniques. Since the inlet and exit annulus area, the mean station diameter, the blade angles, and the velocity diagram of each stage are given in the engine design stage, the efficiency of each stage, computed above, is incorporated to obtain the overall compressor efficiency. The mean work done factor (Refs. (1), (9), (15)) is applied in the analysis to account for the performance deterioration due to velocity profile distortion and the boundary layer development as the flow proceeds downstream in a multi-stage compressor.

5. LOSS THROUGH AXIAL TURBINES

The turbine stage efficiency may be calculated from the estimated values of the stator energy loss, L_s, the rotor energy loss, L_r, and the incidence loss L_i (Refs. (10), (11)).

$$L_s = k_s\left(\frac{C_{in}^2 + C_{out}^2}{2g_cJ}\right) \quad : \quad Stator \tag{3}$$

$$L_r = k_r\left(\frac{W_{in}^2 + W_{out}^2}{2g_cJ}\right) \quad : \quad Rotor \tag{4}$$

Coefficients k_r and k_s represent the profile loss at the design point and are obtained from the Soderberg correlation(Refs. (10), (11)).

$$L_i = \frac{C_{in}^2}{2g_cJ}[1 - \cos^n(i - i_{opt})] \tag{5}$$

$$\begin{cases} n = 2\ (positive\ incidence) \\ n = 3\ (minus\ incidence) \end{cases} \qquad \begin{cases} i_{opt} = -4^\circ \end{cases}$$

The tip clearance loss in terms of η/η_0 may be obtained from Fig. 4 for different tip clearance fraction and degree of reaction. Although the windmilling state is far from the design point the above loss relationships based on the design point data appear to be accurate (Ref. 11).

6. OTHER LOSSES

The air inlet adiabatic efficiency η_i and the engine exhaust nozzle adiabatic efficiency η_N have been assumed to be constant. The total pressure loss of the burner has a significant effect on the results and it is advisable to use the test data, if available. The total temperature of the air stream remains constant in the burner. The mechanical efficiency of turbines has been assumed to be 0.95 and the accessory drive power is assumed to be proportional to the square of the rotational speed (Refs. (13), (14)). It should be pointed out here that widely used loss models were used for this study. However, other loss models can be incorporated into this method as well.

7. MASS FLOW DETERMINATION

The mass flow rate which goes through the engine depends on the axial velocity C_x. Thus, the mass flow rate influences the velocity diagram significantly; the incidence angle and the magnitude of the losses vary accordingly.

The ambient condition P_a, T_a and flight Mach number Ma give the engine inlet total condition P_{T1} and T_{T1}. An initial mass flow is assumed from Eq. (6).

$$\dot{m}_a = \rho V A_i \tag{6}$$

The losses through compressor, turbine and other components are calculated. Using the estimated turbine exit P_T and T_T as the nozzle inlet condition, the nozzle mass flow is calculated and compared with the guessed value. The correct mass flow is obtained by iteration as shown in Fig. 2.

8. TRANSIENT AND STEADY STATE WINDMILLING ANALYSIS

The compressor and turbine torques are calculated from the velocity diagram for the selected rotational speed. The transient windmilling performance is determined from the relationship between compressor and turbine torques.

When the vector sum of these torques becomes zero a steady state windmilling condition is reached and the rotational speed remains constant. The excess turbine torque is expressed by the following relations (Refs. (15), (16)).

$$T_a = T_{a\,turbine} - T_{a\,compressor} - T_{a\,load} \tag{7}$$

The rotor acceleration is then calculated from the following Eq.(8).

$$T_a = I_p \cdot \frac{d\omega}{dt} = 2\pi I_p \cdot \frac{dN}{dt} \tag{8}$$

Calculation steps are shown in detail in Appendix A and sample calculation results are shown in Appendix B.

9. MODEL PREDICTIONS & SENSITIVITY ANALYSIS

A Microturbo TRI 60 engine was chosen as the test engine for this study. TRI 60 is a 900-lb$_f$ thrust class simple turbojet engine having a three-stage axial compressor, a single-stage axial turbine, and a nozzle with 13.8 lbm/s maximum ground static mass flow rate. Approximate geometrical data at the mid-station were obtained from the hardware component measurement and available geometrical information.

A parametric study was carried out to examine the sensitivity of model predictions on various turbine geometric parameters - pitch/chord ratio, turbine blade angles, intake area, turbine inlet area, and exhaust nozzle area. Table 1 shows the model prediction variations from the baseline predictions for ±1% variation in intake area, turbine blade angles, and exhaust nozzle area. When one parameter was varied, all of the other values were held at the baseline (i.e. test engine) values. Overall, the model predictions are

insensitive to small variations in turbine geometry. Therefore, during the preliminary design stage when only approximate geometric data are available, this method can still be used to yield meaningful results. The parametric study actually examined ±10% variation from the baseline configuration.

	Intake Area	Turbine Blade Angle	Exhaust Nozzle Area
RPM	±0.03 %	±1.09 %	±0.22 %
Mass Flow Rate	±0.02 %	∓0.94 %	±0.22 %
Compressor Pressure Ratio	±0.02 %	±0.6 %	±0.06 %
Time to Reach the Steady-State	0.0 %	∓0.35 %	∓0.09 %

Table 1. Results of parametric sensitivity analysis.
(TRI 60, Sea level, International Standard Atmosphere, Ma=0.7, for each 1% variation from baseline geometric data).

10. COMPARISON OF THE ANALYSIS WITH DATA

The model's predictions are compared with the windmilling test data for a TRI 60 engine from Ref. 12. (Figs. 5, 6, and 7). Fig.5 shows steady-state windmilling speed against flight Mach number and altitude. Present method predicts that the steady-state windmilling speed decreases as the flight altitude increases. The altitude data for the TRI 60 engine were not available at the time of this analysis. However, other experimental data (Refs (6), (7)) confirm the trend of the present analysis. Except in the very low flight Mach number region the agreement is satisfactory. Effects of flight Mach number and altitude on the engine mass flow rate is shown in Fig. 6. The agreement between the present analysis and the data is very good for most of the ranges investigated.

Fig. 7 shows the transient windmilling speeds as a function of flight Mach number. The experimental data were available only for a flight Mach number of 0.5. The close agreement of the present analysis with the data at Ma = 0.5 suggests that similar agreement may be expected for other conditions. As the altitude increases, the inertia and mechanical friction of the rotating parts remain essentially constant while the ram energy of the incoming air decreases. Therefore, the time required to reach the steady state windmilling speed is greater at higher altitudes. From Fig. 7 the time required to reach the ignition speed of TRI 60 (4,700~5,300 rpm) and the flight Mach number limit for ignition can be determined.

11. CONCLUSIONS

A practical method of predicting windmilling characteristics of simple turbojet engines has been developed. The loss analysis for each major component, based on the available cascade data correlation, is carried out. The relationship between the compressor torque and the turbine torque determines the windmilling performance. Comparison of the results of the present method with the available TRI 60 turbojet engine test data has shown a good agreement in all of the major windmilling performance parameters.

Present method requires geometric data but does not require any experimental data. Furthermore, approximate geometric values yield meaningful windmilling predictions, and the method is sufficiently flexible to accomodate incorporation of different loss models. Thus, this method can be conveniently used in the early stages of turbojet development.

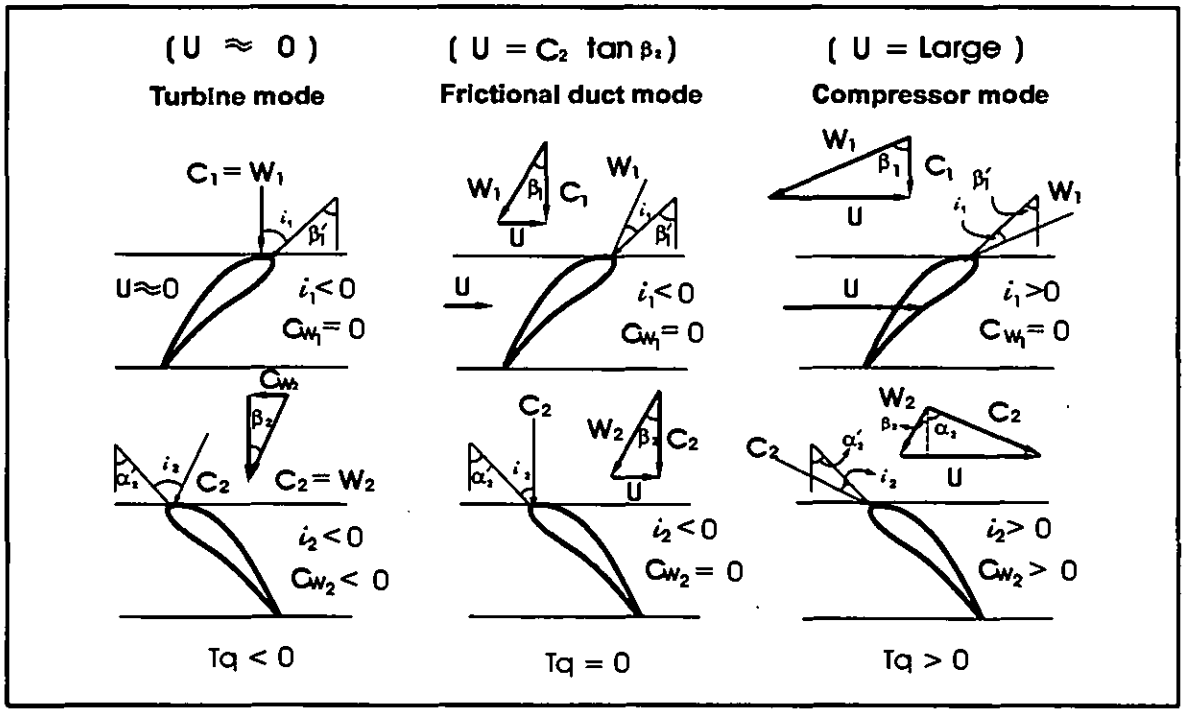

Figure 1: Three different functions of compressor under windmilling condition.

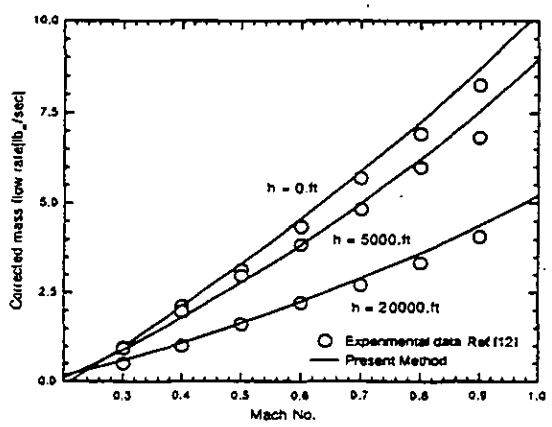

Figure 6: Effects of flight Mach number and altitude on engine mass flow rate under steady state windmilling condition.

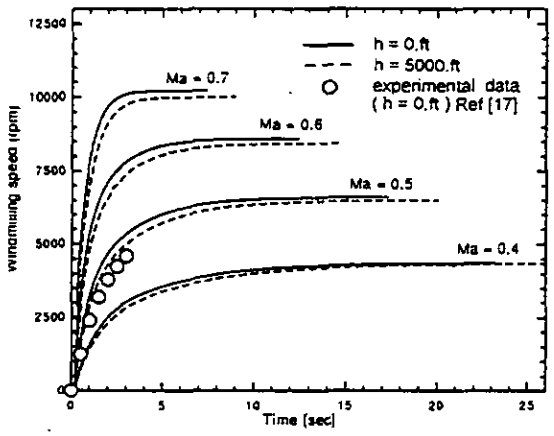

Figure 7: Flight Mach number and transient windmilling speed.

REFERENCES

(1) Hong, Y.S., "Gas Turbine Engines (in Korean)", Cheongmungak Press, Korea, 1983.

(2) Mattingly, J.D., Heiser, W.H., and Daley, D.H., "Aircraft Engine Design", AIAA, INC, 1987.

(3) Kim, S.M., and Hong, Y.S., "A Practical Method for Predicting Part-load Performance of Industrial Gas Turbines (in Korean)", The Korean Society for Aeronautical and Space Sciences, Vol.23, No.3, 1995.

(4) Ainley, D.G., Mathieson, G.C.R., "A Method of Performance Estimation for Axial-Flow Turbines", Report and Memoranda No. 2974, 1951.

(5) Mitsuo Morita, and Makoto Sasaki, "Restart Characteristics of Turbofan Engines", ISABE 89-7127, 9th, 1989, pp. 1200-1206.

(6) Wallner, L.E., and Welna, H.J., "Generalization of Turbojet and Turbine-Propeller Engine Performance in Windmilling Condition", NACA RM E51J23, Dec. 1951.

(7) Sobolushi, A.E., and Farely, J.M., "Steady State Engine Windmilling and Engine Speed Decay Characteristics of Axial Flow Turbojet Engine", NACA RM E51I06, 1951.

(8) Zhao Qi Shou, "Calculation of Windmilling Characteristics of Turbojet Engines", ASME Journal of Engineering for Power, Vol. 103, Jan., 1981, pp. 1-12.

(9) Horlock, J.H., "Axial Flow Compressors", Robert E. Krieger Pub. Co., 1973, pp. 55-60.

(10) Dixon, S.L., "Fluid Mechanics, Thermo-dynamics of Turbomachinery", Pergamon Press, 1978, pp. 67-80.

(11) Ahn, J.C., and Hong, Y.S., "Off-design Performance Prediction of Axial Turbines(in Korean)", Journal of the Korean Society for Aeronautical and Space Sciences, Vol.12, No.3, 1984.

(12) Mischel, C., "TRI 60-3 Typical Engine Performance Computation (KPERF)", Microturbo Co., August, 1986.

(13) Rodgers, C., "Starting Torque Characteristics of Small Aircraft Gas Turbines and APU's", ASME Journal of Engineering for Power, Vol. 102, Apr., 1980, pp. 231-238.

(14) Lancaster, O.E., "Jet Propulsion Engines", Princeton University Press, 1959.

(15) Cohen, H., Rogers G.F.C., and Saravanamutto, H.I.H., "Gas Turbine Theory", Longman, 1972.

(16) Agrawal, R.K., and Yunis, M., "A Generalized Mathematical Model to Estimate Gas Turbine Starting Characteristics", ASME Journal of Engineering for Power, Vol. 104, Jan., 1982, pp. 194-199.

(17) MTSA, "TRI60 ECU Quick Start CEPr Qualification Test", Technical Note No. 0229/94/014, Oct. 1994.

Appendix A

1. Input values

η_i, η_m, η_N, λ, A, A_{in}, A_N, pitch, chord, r_H, r_T, β_1', β_2',
Flight condition(M_a), Ambient condition(P_a, T_a)

2. Calculation of ram effect

$$P_{T1} = \left[1+\eta_i\frac{\gamma-1}{2}M_a^2\right]^{\frac{1}{\gamma-1}}, \qquad T_{T1} = \left[1+\frac{\gamma-1}{2}M_a^2\right]$$

3. Assume initial rpm(N) and mass flow rate(Eq. 6)

Compressor

Calculate the following(Step 4 ~ Step 28) :

4. H, r_m, s/c, $\theta(\beta_1'-\beta_2')$, i, C, T, P, ρ, C_x

5. Nominal deviation ;

$$\delta^* = \frac{500\theta\sqrt{s/c}}{500-\theta\sqrt{s/c}}\left[0.23\left(\frac{2a}{c}\right)^2\frac{\beta_2'}{500}\right]$$

6. Nominal outlet angle : $\beta_2^* = \beta_2'+\delta^*$

7. Nominal incidence : $i^* = \beta_2^*+\varepsilon^*-\beta_1'$

8. Find $\varepsilon/\varepsilon^*$, C_{D_0} from Fig. 2

9. $\beta_2 = \beta_1-\varepsilon$, $\quad \tan\beta_m = \dfrac{\tan\beta_1+\tan\beta_2}{2}$

10. Lift coefficient $C_L = 2(s/c)\cos\beta_m(\tan\beta_1-\tan\beta_2)$

11. C_{Do}, C_{Di} from Eqs. (1), (2).

12. Drag coefficient : $C_D = C_{Do} + C_{Da} + C_{Di}$

13. Total pressure loss : $\Delta P_T = \frac{1}{2} \rho W_1^2 \frac{C_D}{s/c} \frac{\cos^2 \beta_1}{\cos^3 \beta_m}$

14. $\Delta P_{isentropic} = \frac{1}{2} \rho W_1^2 \frac{\tan^2 \beta_1 - \tan^2 \beta_2}{1 + \tan \beta_1}$

15. Stage efficiency : $\eta_{stage} = 1 - \left(\frac{\Delta P_T}{\Delta P_{isentropic}} \right)$

16. Thermodynamic properties(T_T , P_T, ρ) at each stage outlet.

17. Aerodynamic torque at each stage.

$$T_{a(compressor)} = \frac{\dot{m}_a}{g_c} (r_{m2} C_{u2} - r_{m1} C_{u1})$$

Combustor

18. Combustor pressure drop (Experimental Correlation)

Turbine

Stator

19. Velocity components :

$C_x = \dot{m}_a / \rho A$, $C = C_x / \cos \beta$

20. L_s from Eq. (3). $\Delta P_T = \frac{\rho L_s J}{144}$.

21. T_T, P_T, ρ at stator outlet.

Rotor

22. Velocity components : C_x, $W = C_x / \cos \beta$

23. Incidence angle : $i = \beta_1 - \beta_1'$.

24. L_R from Eq. (4). $\Delta P_T = \frac{\rho L_R J}{144}$.

25. L_t from Eq. (5).

26. T_T, P_T, ρ at stator outlet.

27. Aerodynamic torque.

$$T_a = \frac{\dot{m}_a}{g_c} \cdot r_m (C_{u2} - C_{u1})$$

Nozzle

Mass flow rate

28. $\dot{m}_{new} = \frac{P_T A \mathcal{C} (\theta / \theta_{max})}{\sqrt{T_T}}$

where

$$\mathcal{C} = \left(\frac{2}{\gamma + 1} \right)^{\frac{1}{\gamma - 1}} \sqrt{2 \frac{g_c}{R} \frac{\gamma}{\gamma + 1}}$$

$$(\theta / \theta_{max}) = \frac{\left(\frac{P}{P_T} \right)^{\frac{1}{\gamma}} \sqrt{1 - \left(\frac{P}{P_T} \right)^{\frac{\gamma - 1}{\gamma}}}}{\left(\frac{2}{\gamma + 1} \right)^{\frac{1}{\gamma - 1}} \sqrt{\frac{\gamma - 1}{\gamma + 1}}}$$

If $\dot{m}_{new}$ is different from the assumed $\dot{m}_a$ go back to Step 3 and assume a new mass flow rate.

Torque

29. Calculate ΣT_a from Eq.(7)

If $\Sigma T_a \neq 0$, then calculate acceleration time from Eq.(8), and go back to Step 3 and assume a new rpm.

APPENDIX B

Sample calculation results are presented for the TRI60 engine in sea level flight at Mach number of 0.5 with International Standard Atmosphere. The input values are given in Table 2. One mass flow rate iteration (Steps 4–28) at the start of the windmilling process (N=0) is shown in Table 3; though initially assumed to be 3.511, the mass flow rate will converge to a lower value. Table 4 shows compressor and turbine torque calculation steps, after mass flow rate convergence, for N = 923. Since there is excess turbine torque, N is will be increased (Eq. (8)), and the entire calculation process (Figure 2) will be repeated for the new N.

INPUT DATA	
Engine Geometry Data	TRI60 Data
P_a	14.7
T_a	520
M_a	0.5

Table 2. Input data (TRI60 engine, Ma=0.5, Sea level, International Standard Atmosphere).

Station	Step	Results
	Step 3	N = 0 $\dot{m}_a$ = 3.511
The 1st stage compressor rotor	Step 7	i^* = 3.045
	Step 8	$\varepsilon/\varepsilon^*$ = -0.2395 $C_{D,r}$ = 0.0693
	Step 9	β_2 = 8.6271° $\tan\beta_m$ = 0.075845
	Step 12	C_D = 0.0763
	Step 13	ΔP_T = 0.0276
:	:	:
Burner	Step 18	Press. Loss (%) = 13.95
Turbine Stator	Step 20	ΔP_T = 0.067
Turbine Rotor	Step 24	ΔP_T = 0.168
Nozzle	Step 28	P_T = 14.4134 T_T = 546 (θ/θ_{max}) = 0 $\dot{m}_{new}$ = 3.4471

Table 3. Mass flow rate iteration (TRI60 Engine, Ma = 0.5, Sea level, International Standard Atmosphere).

	RESULTS
N(rpm)	923
$\dot{m}_a$(lb_m/sec)	2.755
t(sec)	0.388
T_T(°R)/P_T(psia)	T_{T1}=546.00 P_{T1}=17.29 T_{T2}=545.24 P_{T2}=17.06 T_{T3}=545.24 P_{T3}=15.12 T_{T4}=543.72 P_{T4}=14.86
$T_{q\ compressor}$ (lb_f · ft)	-5.529
$T_{q\ turbine}$ (lb_f · ft)	14.86

{ Sta. 1 : comp. inlet, Sta. 2 : comp. exit
{ Sta. 3 : turb. inlet, Sta. 4 : turb. exit

Table 4. Torque calculation results (TRI60 engine, Ma = 0.5, Sea level, International Standard Atmosphere).